CompAMa
www.compama.co.usb.ve

Bull. Comput. Appl. Math., Vol.5, No.2, 2017
ISSN 2244-8659

Modeling seismic wave propagation using staggered-grid mimetic finite differences

Freysimar Solano-Feo [1], *Juan Guevara-Jordan* [2], *Carlos González-Ramirez* [3], *Otilio Rojas-Ulacio* [4], *Beatriz Otero-Calvinyo* [5]

CompAMa Vol.5, No.2, pp.9-28, 2017 - Accepted April 12, 2017
Special Issue CIMENICS 2016

Abstract

Mimetic finite difference (MFD) approximations of continuous gradient and divergence operators satisfy a discrete version of the Gauss-Divergence theorem on staggered grids. On the mimetic approximation of this integral conservation principle, an unique boundary flux operator is introduced that also intervenes on the discretization of a given boundary value problem (BVP). In this work, we present a second-order MFD scheme for seismic wave propagation on staggered grids that discretized free surface and absorbing boundary conditions (ABC) with same accuracy order. This scheme is time explicit after coupling a central three-level finite difference (FD) stencil for numerical integration. Here, we briefly discuss the convergence properties of this scheme and show its higher accuracy on a challenging

[1]Escuela de Matemáticas, Universidad Central de Venezuela, Caracas, Venezuela (freysimar15@gmail.com).
[2]Escuela de Matemáticas, Universidad Central de Venezuela, Caracas, Venezuela (jmguevarajordan@gmail.com).
[3]Escuela de Matemáticas, Universidad Central de Venezuela, Caracas, Venezuela (carlosl.gonzalez@ciens.ucv.ve).
[4]Escuela de Computación, Universidad Central de Venezuela, Caracas, Venezuela (rojasotilio@gmail.com).
[5]Departamento de Arquitectura de Computadors, Universitat Politécnica de Catalunya, Barcelona, Spain (botero@ac.upc.edu).

test when compared to a traditional FD method. Preliminary applications to 2-D seismic scenarios are also presented and show the potential of the mimetic finite difference method.

Keywords: Acoustic waves, staggered grids, mimetic finite differences, absorbing conditions.

1 Introduction

For Earth models with simple geometry, finite differences (FD) schemes have been widely used for seismic wave propagation given its simple formulation, easy implementation, and low computational cost. A variety of staggered grids (SG) have been employed on FD discretization to achieve accurate results on acoustic and elastic models, even with the inclusion of anisotropic constitutions [1–3]. Some FD schemes have adapted the traditional ghost-point implementation of boundary conditions accounting for certain geometrical complexities [4, 5]. However, finite difference seismic applications still suffer from two main deficiencies: the numerical treatment of boundary conditions is not systematic leading to case dependent approaches that may be highly sensitive to instabilities or inaccuracies and the FD discretization of individual differential operators present on a boundary value problem, leads to a global scheme that do not necessarily preserve the underlying physical principles.

A great improvement on finite difference discretization is due to the extensive work on discrete conservative operators developed in [6]. Two modern finite difference families on staggered grids comes from this pioneering work. The first one is based on the support operators, Divergence D and Gradient G, both providing second-order accuracy at interior grid points, but reduced to first order at domain boundaries. This method has been extensively applied to diffusion, electromagnetic, and viscoelastic problems even on non-uniform meshes [7–9]. The second construction method of conservative operators presents discrete D and G that exhibit second, fourth, and even sixth order accuracy along all grid locations including boundaries. This latter method is introduced in [10], and later reformulated in [11]. For a systematic numerical treatment of Neumann and Robin boundary conditions, authors in [12] develop a new operator B to approximate boundary fluxes of a given vector field. Thus, the numerical solution of a given boundary value

problem based on D, G and B, automatically satisfy a particular discrete version of the fundamental Green-Stoke-Gauss Theorem. This remarkable attribute allows the discrete solution to preserve the conservation properties fulfilled by continuous solutions. As a result, operators D, G and B, have been referred as mimetic. Applications of the mimetic operators D and G to acoustic and elastic wave propagation can be found in [13–15]. In the last reference, an implementation of free surfaces (FS) on 3-D deformed grids allows accounting for realistic topography, and outgoing waves are damped thanks to efficient absorbing boundary conditions. Another applications of D and G concern the frictional propagation of shear ruptures on embedding elastic media [16, 17]. Even though these methods show accurate results on seismic applications, their formulation lack of the boundary operator B, therefore those are not mimetic schemes.

Recently, [18] proposed a new discretization of the acoustic wave equation on 1-D and 2-D domains based on the three mimetic operators D, G and B. Spatial discretization in [18] is limited to second order accuracy, but these mimetic formulation and convergence analysis are easily extensible to the case of four-order schemes, that are commonly used on seismic modeling. In this work, we review the methodology proposed in [18] and presents new interesting applications in one and two dimensions.

This paper is organized in the following way: Section 2 presents formulations of the acoustic wave equation of seismic interest in 1-D and 2-D media. Section 3 gives a brief review of 1-D mimetic discretization operators. In section 4, we discuss the formulation of a fully mimetic method for acoustic motion on 1-D and 2-D rectangular staggered grid. The combined operator DG approximates the Laplacian at interior grid nodes, while BG allows the implementation of free surface and absorbing boundary conditions at grid edges. Remarkably, the operator BG also adds a significant contribution to the Laplacian at grid points neighbors to boundary lines. A convergence analysis of these schemes are also discussed in this section. Section 5 presents the application of our 1-D mimetic method to a numerical test that exhibits strong gradients at edges, in addition to a comparison against a ghost-point based finite difference scheme. Next (see section 6), two interesting 2-D tests are given in section 6 where satisfactory results are observed. The first test involves a homogeneous velocity model, while the second one considers a three-layered heterogeneous medium with horizontal stratification. These tests are used to assess the efficiency of Reynold absorbing boundary conditions [19] by comparing wave patterns under rigid boundaries. Conclusions

and some guidelines for future works are given in section 7.

2 The acoustic wave equation

In this work, we model seismic motion by means of the acoustic wave equation written in a second order differential formulation. The mimetic discretization proceeds on a staggered grid and for this reason the discrete solution and its spatial gradients are placed at different grid locations shifted by half of the spacing. This fact renders higher accuracy to the staggered grid differentiation as compared to traditional finite difference methods based on nodal grids.

2.1 1-D formulation

In a 1-D acoustic medium, the particle displacement satisfy the following equation

$$\frac{\partial^2 u}{\partial t^2} - c^2 \frac{\partial^2 u}{\partial x^2} = f(x,t), \tag{1}$$

where c represents the wave speed and $f(x,t)$ is the source term. In the following sections, we assume that $x \in [0,a]$, $t \geq 0$, and the initial condition is $u(x,0) = \frac{\partial u}{\partial t} = 0$. We also consider boundary conditions of the form

$$\frac{\partial u}{\partial x}(0,t) = f_1(t), \tag{2}$$

$$\left[\frac{\partial u}{\partial t} + c\frac{\partial u}{\partial x}\right](a,t) = f_2(t). \tag{3}$$

In the case when $f_1(t) = f_2(t) = 0$, Eq. (2) represents a free surface (FS) Neumman-type boundary condition, while Eq. (3) models outgoing waves through $x = a$ that Reynolds [19] defines as a first order absorbing operator.

2.2 2-D formulation

In seismic applications, the propagation of primary (P) waves satisfy a multi-dimensional version of above formulation (1). In this work, we only consider the following wave propagation model on a 2-D rectangular domain

$$\frac{\partial^2 u}{\partial t^2} - c^2 \nabla^2 u = f(x,z,t), \qquad (x,z) \in [0,a] \times [0,b], \tag{4}$$

where u represents the acoustic pressure. In this equation, ∇^2 is the Laplacian operator, and similarly to the 1-D case c and f denotes the wave speed and the seismic source, respectively. In this case, we associate the rectangle edges $x = 0$, $x = a$ and $z = b$ to artificial absorbing boundary conditions, and consider the boundary $z = 0$ as a free surface. Thus,

$$\left(\frac{\partial u}{\partial t} - c\frac{\partial u}{\partial x}\right)(0, z, t) = 0, \tag{5}$$

$$\left(\frac{\partial u}{\partial t} + c\frac{\partial u}{\partial x}\right)(a, z, t) = 0, \tag{6}$$

$$\left(\frac{\partial u}{\partial t} + c\frac{\partial u}{\partial z}\right)(x, b, t) = 0, \tag{7}$$

$$u(x, 0, t) = 0. \tag{8}$$

It is appropriate to note, that the free surface boundary (8) is given as a Dirichlet condition.

3 Review of 1-D mimetic discretization

The mimetic finite difference discretization of a boundary value problem in the spatial domain proceeds by substituting the continuous differential operators gradient (∇), divergence ($\nabla\cdot$) and the normal derivative ($\frac{\partial}{\partial \vec{n}}$) at boundaries by the discrete versions G, D, and B proposed in [12] and [10]. These mimetic operators satisfy the following approximation to the Green's Identity

$$\langle Dv, u\rangle_Q + \langle v, Gu\rangle_P = \langle Bv, u\rangle_I , \tag{9}$$

with the weighted inner product $\langle\cdot,\cdot\rangle_A$ defined by

$$\langle x, y\rangle_A = x^t A y, \qquad x, y \in \mathbb{R}^n,$$

where A is a positive definite matrix. In this case, I represents the identity matrix, Q and P are weight diagonal matrices whose elements agree with the coefficients of mid-point quadrature and $\frac{3}{8}$ Newton-Cotes quadrature, respectively. The above discrete principle (9) holds because the boundary flux operator is given by

$$B = QD + G^t P. \tag{10}$$

The matrix representations of operators D, G and B depend on the discretization of scalar and vector fields u and v, respectively. In the 1-D case, Castillo and collaborators discretized the domain $[0, a]$ by using uniform cells $[x_i, x_{i+1}]$ with nodes $x_i = ih$ for $i = 0, \ldots, n$ and grid step $h = \frac{a}{n}$. This grid becomes staggered by including the cell centers $x_{i+\frac{1}{2}} = \frac{x_i + x_{i+1}}{2}$. Discrete values of the function u are considered at cell centers $x_{i+\frac{1}{2}}$ in addition to the boundary values at x_0 and x_n. Evaluations of the function v are placed only at grid nodes. For simplicity, Figure 1(a) just depicts the grid distribution of discrete u values which are collected in the vector $\vec{u}$. Similarly, a vector $\vec{v}$ allows storing evaluations of the field v.

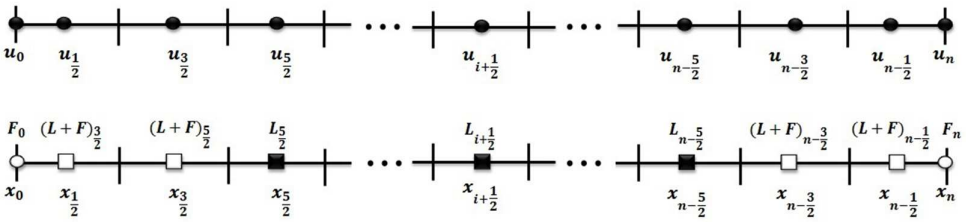

Fig. 1: 1-D staggered grid for discretization of function u using mimetic operators B, G and D. The operator $L = DG$ is the Laplacian discretization and $F = BG$ arises from the approximation of boundary conditions.

Numerical differentiation of u is computed by $G\vec{u}$, which renders $n+1$ approximations to $\frac{du}{dx}$ at each grid node. In the same way, $D\vec{v}$ yields approximations of $\frac{dv}{dx}$ at the n cell centers. Second order accurate mimetic gradient and divergence operators are given by

$$G = \frac{1}{h} \begin{pmatrix} -\frac{8}{3} & 3 & -\frac{1}{3} & 0 & \ldots & 0 \\ 0 & -1 & 1 & 0 & \ldots & 0 \\ \vdots & & \ddots & \ddots & & \vdots \\ 0 & \ldots & 0 & -1 & 1 & 0 \\ 0 & \ldots & 0 & \frac{1}{3} & -3 & \frac{8}{3} \end{pmatrix},$$

$$D = \frac{1}{h}\begin{pmatrix} 0 & 0 & 0 & 0 & \dots & 0 \\ -1 & 1 & 0 & 0 & \dots & 0 \\ \vdots & & \ddots & \ddots & & \vdots \\ 0 & \dots & 0 & 0 & -1 & 1 \\ 0 & 0 & 0 & 0 & \dots & 0 \end{pmatrix}$$

The first and last rows of G corresponds to lateral discretization of boundary values of $\frac{du}{dx}$, which coincide with the Taylor-based FD-SG stencils. The remaining rows of G, as well as non-zero rows of operator D are given by the classical staggered grid central formula for differentiation at interior mesh points with a second order accuracy. Authors in [10,11] constructed higher-order versions of these differential operators and methods given in next section could be easily be extended accordingly. On the other hand, the mimetic operator D exhibits first and last zero rows to allow a convenient accommodations of Neumann or Robin boundary conditions, as we show in next section.

According to above expressions for D and G, the flux operator B follows from Eq.(10)

$$B = \begin{pmatrix} -1 & 0 & 0 & & \dots & & 0 \\ \frac{1}{8} & -\frac{1}{8} & 0 & & \dots & & 0 \\ -\frac{1}{8} & \frac{1}{8} & 0 & & \dots & & 0 \\ 0 & 0 & 0 & & \dots & & 0 \\ \vdots & \vdots & \vdots & \ddots & \vdots & \vdots & \vdots \\ 0 & & \dots & & 0 & -\frac{1}{8} & \frac{1}{8} \\ 0 & & \dots & & 0 & \frac{1}{8} & -\frac{1}{8} \\ 0 & & \dots & & 0 & 0 & 1 \end{pmatrix}.$$

Notice that the first and last rows in B represent the outward normal vector at grid boundaries, thus the same rows in the composed operator BG allows approximating $\frac{\partial u}{\partial \vec{n}}$ at these edges (denoted as F in Figure 1(b)). The non zero interior rows of B add an important contribution to the Laplacian approximation $L = DG$ at the two nearest cell centers to each grid boundary

(denoted as $F+L$ in Figure 1(b)). The remaining zero rows in B do not affect Laplacian calculations at interior cell centers (as also shown by Figure 1(b)).

4 Mimetic finite difference schemes for acoustic wave propagation.

4.1 1-D case.

Based upon the matrix structure of MFD operators given above, here we present the discrete iterative formulas that conform our 1-D scheme. Let $u^k_{i+\frac{1}{2}}$ denotes the discrete pressure at time $t = k\Delta t$ and cell center $x_{i+\frac{1}{2}}$, where Δt represents the time step. We apply standard central differentiation in time and the MFD discretization of Laplacian $L_{i+\frac{1}{2}}$ for $i = 2, \ldots, n-2$ to write

$$\frac{u^{k+1}_{i+\frac{1}{2}} - 2u^k_{i+\frac{1}{2}} + u^{k-1}_{i+\frac{1}{2}}}{\Delta t^2} = \left(\frac{c}{h}\right)^2 \left[u^k_{i+\frac{3}{2}} - 2u^k_{i+\frac{1}{2}} + u^k_{i-\frac{1}{2}}\right]. \tag{11}$$

This equation represents the mimetic scheme at interior cell centers, but grid points $x_{\frac{1}{2}}$ and $x_{\frac{3}{2}}$ require of using the following lateral mimetic approximations for the Laplacian

$$(L+F)_{\frac{1}{2}} = \left(\frac{8c^2}{3h^2} - \frac{c}{3h}\right)u^k_0 + \left(\frac{c}{2h} - \frac{4c^2}{h^2}\right)u^k_{\frac{1}{2}} + \left(\frac{4c^2}{3h^2} - \frac{c}{6h}\right)u^k_{\frac{3}{2}}, \tag{12}$$

$$(L+F)_{\frac{3}{2}} = \left(\frac{c}{3h}\right)u^k_0 + \left(\frac{c^2}{h^2} - \frac{c}{2h}\right)u^k_{\frac{1}{2}} + \left(\frac{c}{6h} - \frac{2c^2}{h^2}\right)u^k_{\frac{3}{2}} + \left(\frac{c^2}{h^2}\right)u^k_{\frac{5}{2}} \tag{13}$$

After coupling these singular Laplacian stencils to the same three-step time discretization used before, the method update equations at cell centers $x_{\frac{1}{2}}$ and $x_{\frac{3}{2}}$ are fully stated. Discrete equations at $x_{n-\frac{1}{2}}$ and $x_{n-\frac{3}{2}}$ are analogous, so we omit them. A similar procedure is followed at the boundary point x_0 where discretization in space comes from the contribution of both the flux and gradient operators

$$F_0 = -\frac{8}{3h}u^k_0 + \frac{3}{h}u^k_{\frac{1}{2}} - \frac{1}{3h}u^k_{\frac{3}{2}}. \tag{14}$$

Lastly, the discretization of the absorbing boundary conditions at node x_n (3), is given by using a step-forward difference for the time variable combined

to a similar discretization of (14), with a sign change given by the outward normal at $x = a$.

A formal consistency and stability analysis of this mimetic scheme is given in [18], and here we only discuss some singular related facts. The discrete updating equations for both boundary conditions, as well as those applied at centers $x_{i+\frac{1}{2}}$ for $i = 2, \ldots, n-2$, present quadratic truncation errors in space. The spatial discretization degrades to first order only for the cases of the Laplacian approximations at $x_{\frac{1}{2}}$ and $x_{\frac{3}{2}}$ where Taylor expansions yields to

$$(L+F)_{\frac{1}{2}} - c^2 \frac{\partial^2 u}{\partial x^2}(x_{\frac{1}{2}}) = \frac{1}{8} h \frac{\partial^2 u}{\partial x^2}, \quad (L+F)_{\frac{3}{2}} - c^2 \frac{\partial^2 u}{\partial x^2}(x_{\frac{3}{2}}) = -\frac{1}{8} h \frac{\partial^2 u}{\partial x^2}. \quad (15)$$

The study of truncation errors at symmetric locations $x_{n-\frac{1}{2}}$ and $x_{n-\frac{3}{2}}$ is analogous. Thus, our 1-D mimetic scheme is formally $O(h)$. On the other hand, a stability analysis under periodic boundary conditions and based on the eigenvalue estimation of the amplification matrix proved that this scheme is stable for a limiting Courant value of $\frac{c\Delta t}{h} < \frac{\sqrt{3}}{2}$. As a reference basis, we also implement a traditional finite difference method based on the same time discretization and using the interior Laplacian approximations at all cell centers $L_{\frac{3}{2}}$,...,$L_{n-\frac{3}{2}}$ (i.e., omitting BG interior contributions and just leaving the standard central FD). However, we had follow Strickwerda (section 8.2 in [20]) to implement the free surface condition by adding the ghost or imaginary cell center $x_{-\frac{1}{2}} = -\frac{h}{2}$ to the 1-D staggered grid. Then, we use the interior discrete update (11) at $x_{\frac{1}{2}}$ with grid step $\frac{h}{2}$, and substitute imaginary $u_{-\frac{1}{2}}$ in terms of u_0 and $u_{\frac{1}{2}}$ by means of a second order average. Thus, the mimetic calculation at the free surface boundary (14) is now replaced by

$$\frac{u_0^{k+1} - 2u_0^k + u_0^{k-1}}{\Delta t^2} = \left(\frac{c}{h}\right)^2 \left[4u_{\frac{1}{2}}^k - 8u_0^k + 4u_{-\frac{1}{2}}^k\right]. \quad (16)$$

The remaining updating equations of this ghost-point based FD scheme at locations $x_{\frac{1}{2}}$,$x_{n-\frac{1}{2}}$, and x_n are given in [18]. This method is also formally $O(h)$, and presents a Courant limit of $\frac{c\Delta t}{h} < \frac{1}{2}$ under same boundary conditions, which reveals its higher stability restriction compared to the mimetic finite difference method.

4.2 2-D case.

The extension of the mimetic mesh to 2-D or 3-D rectangular domains is obtained as the tensor product of the one-dimensional grid in each coordinate direction, after omitting the corner points. Figure 2 presents the 2-D grid for the mimetic discretization. The gradient operator is now a vector with two components G_x and G_z, which are computed at the mid point of the four edges of every grid block, as depicted in panel (a) with star symbols. Thus, gradient components are also defined at boundaries along with the discrete solution u, and it is shown by circles in panel (b). In addition, the grid presents u values at the center of every cell as illustrated by square symbols. These grid locations also hold the evaluations of the divergence operator D, that is only defined at domain's interior as depicted in both panels. Finally, panel (b) presents grid locations of main operators of a 2-D mimetic discretization. The implementation of boundary conditions by means of the flux operator $F = BG$ is carried out at circles. The contribution of F is added to the Laplacian $L = DG$ approximation at near-boundary (empty) square points. The computation of the standard Laplacian in finite difference is performed at interior (filled) square centers.

Next, we present some details of the mimetic discretization of the 2-D wave equation (4) to (8). Without loss of generality, a common grid spacing h is assumed on both directions, and we consider an uniform partition of $N_x \times N_z$ cells of the domain $\mathcal{D}$, with N_x grid intervals along the x axis, and N_z grid intervals along the z axis. The time step is again denoted by Δt. On this grid, u_{ij}^k is the numerical approximation of $u(x_i, z_j, t_k)$, and (x_i, z_j) is one of the boundary or mid-cell points illustrated on Figure 2 in panel (b). Because of the 2-D mimetic scheme is not a complex generalization of the one-dimensional case, we only present the discrete updating stencils at certain mesh points. The first three cases correspond to calculations at boundary points and cell centers nearby. By symmetry and after a sign change, the counterpart update equations at remaining edges and neighbor points can be written in the same way.

(i) Node $\circ$: $u(x_i, z_j)$ for $i = 0$ and $j \in \{\frac{1}{2}, \ldots, N_z - \frac{1}{2}\}$,

$$u_{ij}^{k+1} = u_{ij}^k + \left(\frac{c\Delta t}{h}\right)\left[-\tfrac{8}{3}u_{ij}^k + 3u_{i+\frac{1}{2}j}^k - \tfrac{1}{3}u_{i+\frac{3}{2}j}^k \right].$$

(ii) Node □: $u(x_i, z_j)$ for $i \in \{\frac{1}{2}, N_x - \frac{1}{2}\}$ and $j \in \{\frac{1}{2}, N_z - \frac{1}{2}\}$,

$$u_{ij}^{k+1} = 2u_{ij}^k - u_{ij}^{k-1} + \Delta t^2 \left[\left(\frac{8c^2}{3h^2} - \frac{c}{3h} \right) u_{i-\frac{1}{2},j}^k + \left(\frac{c}{2h} - \frac{6c^2}{h^2} \right) u_{i,j}^k + \left(\frac{4c^2}{3h^2} - \frac{c}{6h} \right) u_{i\pm 1,j}^k + \left(\frac{c^2}{h^2} \right) u_{i,j+1}^k + \left(\frac{c^2}{h^2} \right) u_{i,j-\frac{1}{2}}^k \right].$$

(iii) Node □: $u(x_i, z_j)$ for $i \in \{\frac{3}{2}, N_x - \frac{3}{2}\}$ and $j \in \{\frac{5}{2}, \ldots, N_z - \frac{5}{2}\}$,

$$u_{ij}^{k+1} = 2u_{ij}^k - u_{ij}^{k-1} + \Delta t^2 \left[\left(\frac{c^2}{h^2} - \frac{c}{2h} \right) u_{i\mp 1,j}^k + \left(\frac{c}{6h} - \frac{4c^2}{h^2} \right) u_{i,j}^k + \left(\frac{c}{3h} \right) u_{i-\frac{3}{2},j}^k + \left(\frac{c^2}{h^2} \right) u_{i\pm 1,j}^k + \left(\frac{c^2}{h^2} \right) u_{i,j-1}^k + \left(\frac{c^2}{h^2} \right) u_{i,j+1}^k \right].$$

(iv) Node ■: $u(x_i, z_j)$ for $i \in \{\frac{5}{2}, \ldots, N_x - \frac{5}{2}\}$ and $j \in \{\frac{5}{2}, \ldots, N_z - \frac{5}{2}\}$,

$$u_{ij}^{k+1} = 2u_{ij}^k - u_{ij}^{k-1} + \left(\frac{c\Delta t}{h} \right)^2 \left[u_{i-1,j}^k + u_{i+1,j}^k - 4u_{ij}^k + u_{i,j-1}^k + u_{i,j+1}^k \right].$$

5 A 1-D convergence test.

The goal of this section is assessing the accuracy and empirical convergence of our 1-D mimetic scheme on a numerical tests whose continuous solutions exhibit significant gradients at $x = 0$. For comparison purposes, we also solve this test using the ghost-point based finite difference method described in section 4.1. We set up initial and boundary conditions in the wave model (1)-(3) in such a way that the exact solution corresponds to

$$u(x,t) = \cos(2\pi x)[\sin(2\pi t) + \cos(2\pi t)]e^{-\alpha x}, \tag{17}$$

and choose $x \in [0,1]$ and $0 \leq t \leq 1$ as the problem's domain. Notice that α is the control parameter for the mild solution boundary layer at $x = 0$. Figure 3 depicts the absolute L_2 errors of both mimetic and traditional finite difference solutions for sixteen grid sizes in the range $n = 40$ to $n = 120$ in

jumps of five, and using a common time step $\Delta t = 0.55h$. In our experiments, we observe higher accuracy on mimetic results for α values above 25, but we only show one representative case corresponding to $\alpha = 37$. Notice that the finite difference scheme yields a L_2 error at the finest grid, which is nearly the same achieved by the mimetic scheme at $n = 95$. This represents a 20% memory saving and also implies a reduction on the computing cost. This computational advantage is minor on coarser grids, and arises from the faster (almost quadratic) mimetic convergence. It is important to remark that the formal $O(h)$ truncation errors of Laplacian near-boundary mimetic discretization, do not affect the practical convergence on this hard problem. On the other hand, the traditional scheme with a proven quadratic convergence delivers superlinear rates at the most. Convergence rate (CR) give on legend of Figure 3 correspond to linear-square fittings of quantified errors.

6 Simulations on 2-D media

In this section, we present two numerical tests where shallow point sources induce seismic motion that we record on surface receivers. The first one is an homogeneous squared medium, and the tests involves a three-layered rectangular model with horizontal stratification. In both tests, we have used only the new mimetic scheme under two different types of boundary conditions.

6.1 A homogeneous velocity model

This numerical test is based upon the research undertaken by Reynolds in [19] where an homogeneous medium is perturbed by a Ricker source located at 37m below the surface. This cross section is square with a lateral extension of 488m and constant P-wave speed of 1500 m/s. Figure 4(a) shows this simple Earth model, and Figure 4(b) depicts the staggered grid used on our numerical calculations. This grid is uniform with 500×500 total evaluations of the discrete solutions. Wave patterns are recorded by one hundred receptors located at the top of the model (free surface), each of them with a separation of 5m from its neighbors.

On this model, we numerically solve two different boundary problems, both with a free surface at the top edge. The first problem considers first order Reynolds' absorbing boundary conditions at the bottom and lateral edges, to model the expected behavior of seismic waves. The second problem

replaces the absorbing boundary condition by Rigid-wall conditions as a way to assess the efficiency of the former absorbing techniques. Seismic traces of the first problem can be observed in Figure 5(a) where one can appreciate only the arrival of the direct wave triggered by the source point. On the other hand, on solutions to the second problem reflected waves arriving at times 0.1s and 0.2s respond to the fact that direct waves bounce off of the lateral walls which are shown in Figure 5(b).

6.2 A layered velocity model.

This problem is based on the model given in [21] with variable wave speed as shown in Figure 6(a). This earthbound model corresponds to a rectangular section with dimensions 300m long (horizontal direction) and 150m deep (vertical direction). This cross section is splitted into three layers with horizontal stratification with speeds given in Figure 6(a). As is specified in Figure 6(a), this region is covered by a uniform distributed staggered grid with a total of 300×150 discrete evaluations of the unknown solution (square cells with 1m edge size). In this model, we use a point source located at the center of the x dimension and near from the top boundary, generating a signal which is later received by 100 geophones located at the top of the terrain and separated by 3m from each other. In order to study the behavior of excited waves, we analyze seismic traces obtained in both boundary problems used in the homogeneous case (Figure 6(b)).

The seismic traces corresponding to this boundary problem are show in Figure 7(a). The first wave obtained between initial time and 0.05s corresponds to the direct wave generated by the source term. The primary wave corresponding to the first layer, which is located 48m deep from the source, has an arrival time of 0.077s. On the other hand, the arrival time of the secondary wave is 0.12s, which corresponds to the rebounds generated by the collision of first wave with the multiple layers. Seismic traces are in consistency with [21]. After 0.12s of simulation, seismic traces shows little reflections as a consequence of the first order absorbing boundary conditions. With the purpose of compare the effectiveness of boundary conditions, we have considered a second problem with Dirichlet type boundary conditions based on expressions (8), and their traces are show in Figure 7(b). The simulation time in both problems is 0.15s and the time step is taken as $\Delta t = (0.55)h/c_{max}$, where c_{max} represents the highest wave speed of the model.

7 Conclusions

We present a new numerical scheme based on second order mimetic finite differences to solve the seismic wave equation under a combination of different boundary conditions. A formal convergence analysis proves that the mimetic scheme has an stability range $\sqrt{3}$ times larger than the limit of a traditional finite difference method under the same boundary conditions. Respect to the same method, the mimetic scheme delivers more accurate numerical results that converge almost quadratically to exact solutions with extreme gradients at boundaries. On 2-D seismic scenarios, the results of this mimetic scheme are good and physically consistent with expected wave patterns on both homogeneous and heterogeneous domains. Currently, absorbing boundaries are based on the first-order Reynolds operators, however we plan to enhance this implementation feature by using higher-order operators or related techniques. For future works, we also want to extend and apply the mimetic scheme to three-dimensional seismic models.

Acknowledgements

This research was supported by Consejo de Desarrollo Científico y Humanístico, Universidad Central de Venezuela.

References

[1] J. Etgen and M. O'Brien. Computational methods for large-scale 3d acoustic finite-difference modeling: A tutorial. *Geophysics*, 72(5):SM223–SM230, 2007. DOI: 10.1190/1.2753753.

[2] P. Moczo, J. Robertsson, and L. Eisner. The finite-difference time-domain method for modeling of seismic wave propagation. *Advances in Geophysics*, 48:421–516, 2007. DOI: 10.1016/S0065-2687(06)48008-0.

[3] H. Yan and Y. Liu. High-order finite-difference numerical modeling of wave propagation in viscoelastic tti media using rotated staggered grid. *Chinese Journal of Geophysics*, 55(2):252–265, 2012. DOI: 10.1002/cjg2.1719.

[4] R. Graves. Simulating seismic wave propagation in 3d elastic media using staggered-grid finite differences. *Bulletin of*

the Seismological Society of America, 86(4):1091–1106, 1996. http://www.bssaonline.org/content/86/4/1091.short.

[5] C. Gélis, D. Leparoux, J. Virieux, A. Bitri, S. Operto, and G. Grandjean. Numerical modeling of surface waves over shallow cavities. *Journal of Environmental & Engineering Geophysics*, 10(2):111–121, 2005. DOI: 10.2113/JEEG10.2.111.

[6] A. Samarskii, V. Tishkin, A. Favorskii, and M. Shashkov. Operational finite-difference schemes. *Differential Equations*, 17(7):854–862, 1981. DOI:.

[7] D. Steven, G. Ely, and J. Minster. A support-operator method for viscoelastic wave modelling in 3-d heterogeneous media. *Geophysical Journal International*, 172(1):331–344, 2008. DOI: 10.1111/j.1365-246X.2007.03633.x.

[8] J. Hyman and M. Shashkov. Mimetic finite difference methods for Maxwell's equations and the equations of magnetic diffusion. *Progress in Electromagnetics Research*, 32:89–121, 2001. www.jpier.org/PIER/pier32/04.00080104.shashkov.pdf.

[9] J. Hyman, M. Shashkov, and S. Steinberg. The numerical solution of diffusion problems in strongly heterogeneous non-isotropic materials. *Journal of Computational Physics*, 132(1):130–148, 1997. DOI: 10.1006/jcph.1996.5633.

[10] J. Castillo, J. Hyman, M. Shashkov, and S. Steinberg. Fourth-and sixth-order conservative finite difference approximations of the divergence and gradient. *Applied Numerical Mathematics*, 37(1):171–187, 2001. DOI: 10.1016/S0168-9274(00)00033-7.

[11] J. Castillo and R. Grone. A matrix analysis approach to higher-order approximations for divergence and gradients satisfying a global conservation law. *SIAM Journal on Matrix Analysis and Applications*, 25(1):128–142, 2003. DOI: 10.1137/S0895479801398025.

[12] J. Castillo and M. Yasuda. Linear systems arising for second-order mimetic divergence and gradient discretizations. *Journal of Mathematical Modelling and Algorithms in Operations Research*, 4(1):67–82, 2005. DOI: 10.1007/s10852-004-3523-1.

[13] O. Rojas, B. Otero, J. Castillo, and S. Day. Low dispersive modeling of Rayleigh waves on partly staggered grids. *Computational geosciences*, 18(1):29–43, 2014. DOI: 10.1007/s10596-013-9380-0.

[14] J. De la Puente, M. Ferrer, M. Hanzich, J. Castillo, and J. Cela. Mimetic seismic wave modeling including topography on deformed staggered grids. *Geophysics*, 79(3):T125–T141, 2014. DOI: 10.1190/geo2013-0371.1.

[15] L. Córdova, O. Rojas, B. Otero, and J. Castillo. Compact finite difference modeling of 2-d acoustic wave propagation. *Journal of Computational and Applied Mathematics*, 295:83–91, 2016. DOI: 10.1016/j.cam.2015.01.040.

[16] O. Rojas, D. Steven, J. Castillo, and L. Dalguer. Modelling of rupture propagation using high-order mimetic finite differences. *Geophysical Journal International*, 172(2):631–650, 2008. DOI: 10.1111/j.1365-246X.2007.03651.x.

[17] O. Rojas, E. Dunham, S. Day, L. Dalguer, and J. Castillo. Finite difference modelling of rupture propagation with strong velocity-weakening friction. *Geophysical Journal International*, 179(3):1831–1858, 2009. DOI: 10.1111/j.1365-246X.2009.04387.x.

[18] F. Solano-Feo. Un esquema mimético en diferencias finitas para la ecuación de onda acústica. Master's thesis, Facultad de Ciencias, Universidad Central de Venezuela, 2016.

[19] A. Reynolds. Boundary conditions for the numerical solution of wave propagation problems. *Geophysics*, 43(6):1099–1110, 1978. DOI: 10.1190/1.1440881.

[20] J. Strikwerda. *Finite difference schemes and partial differential equations*. Siam, 2004. ISBN: 978-0-89871-567-5.

[21] D. Keiswetter, R. Black, and C. Schmeissner. A program for seismic wavefield modeling using finite-difference techniques. *Computers & Geosciences*, 22(3):267–286, 1996. DOI: 10.1016/0098-3004(95)00078-X.

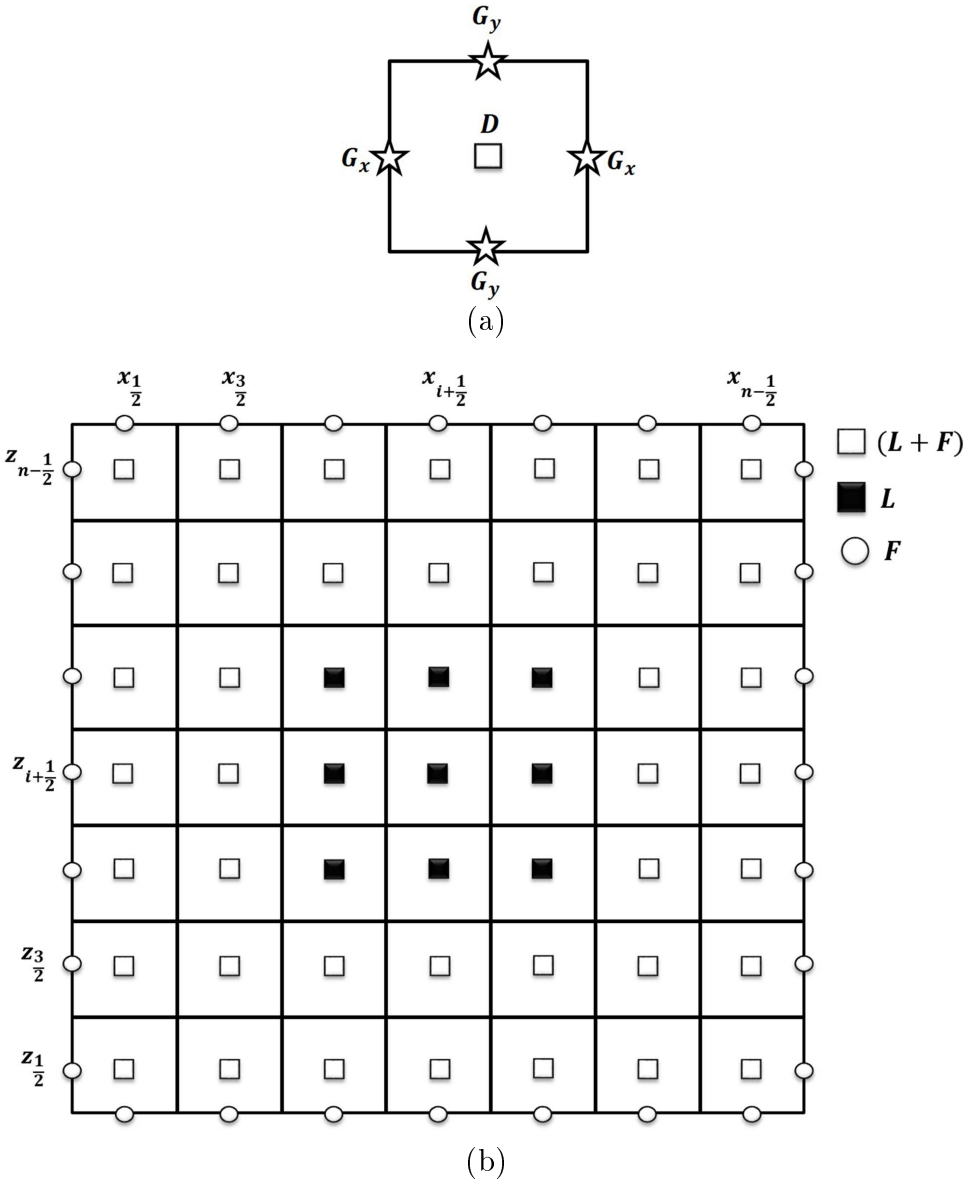

Fig. 2: 2-D grid for MFD discretization. A generic cell with calculations of G_x, G_z, and D is shown in panel (a). Panel (b) illustrates the computation of the flux operator F, $L+F$ and the laplacian operator L.

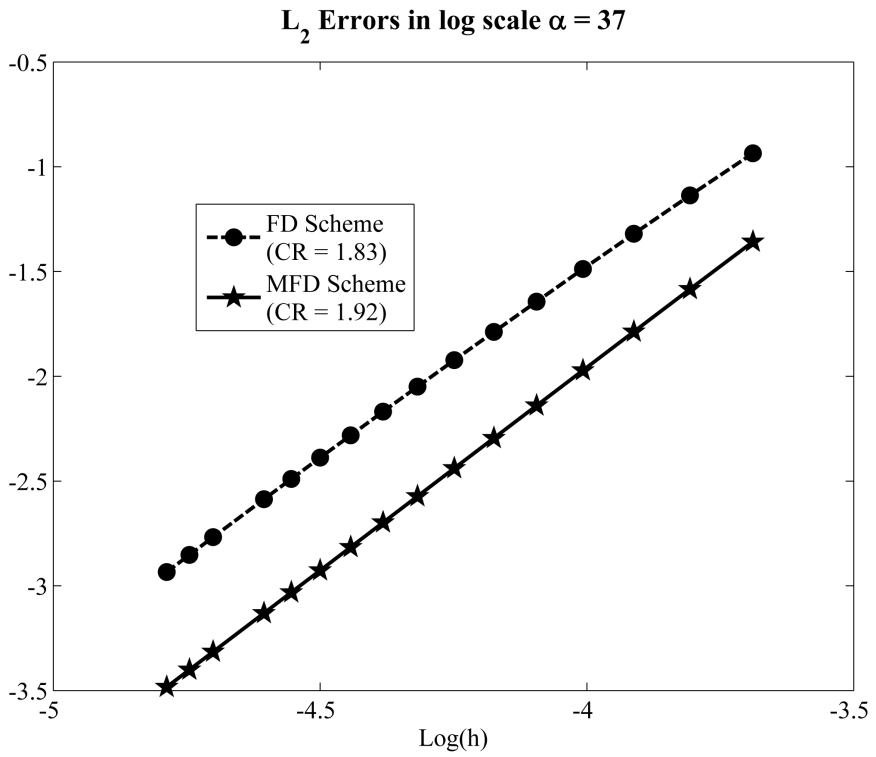

Fig. 3: Absolute L_2 errors of MFD and traditional FD solutions to the 1-D test problem described in section 5 for $\alpha = 37$. Fitted convergence rates (CR) are given on corresponding legend.

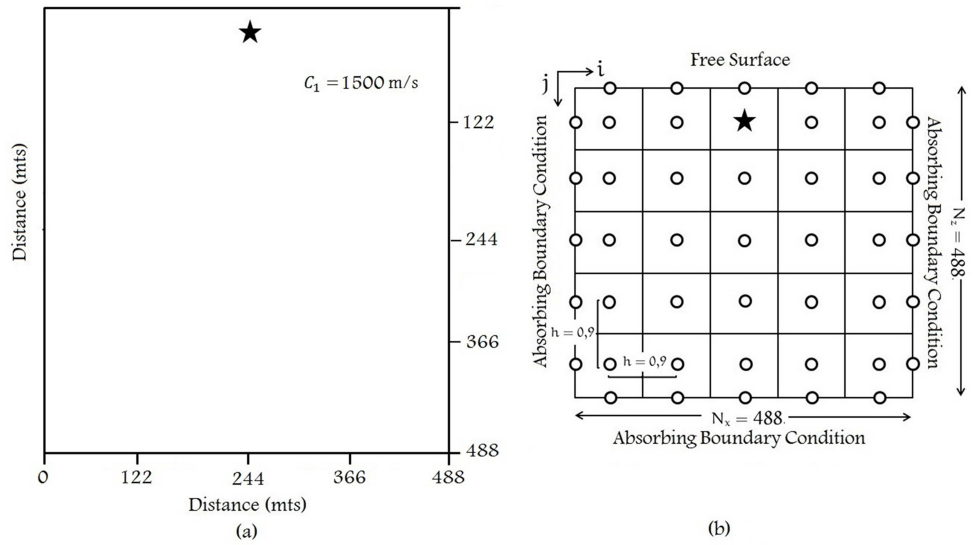

Fig. 4: (a) A homogeneous and square velocity model. (b) Computational region with a staggered grid. The star symbol represents the seismic source point.

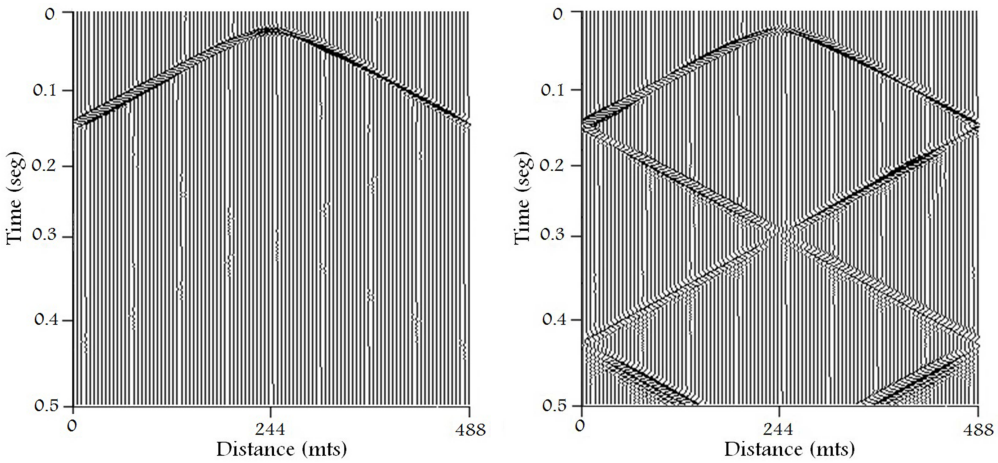

Fig. 5: (a) Seismic traces for absorbing conditions. (b) Seismic traces for Dirichlet conditions.

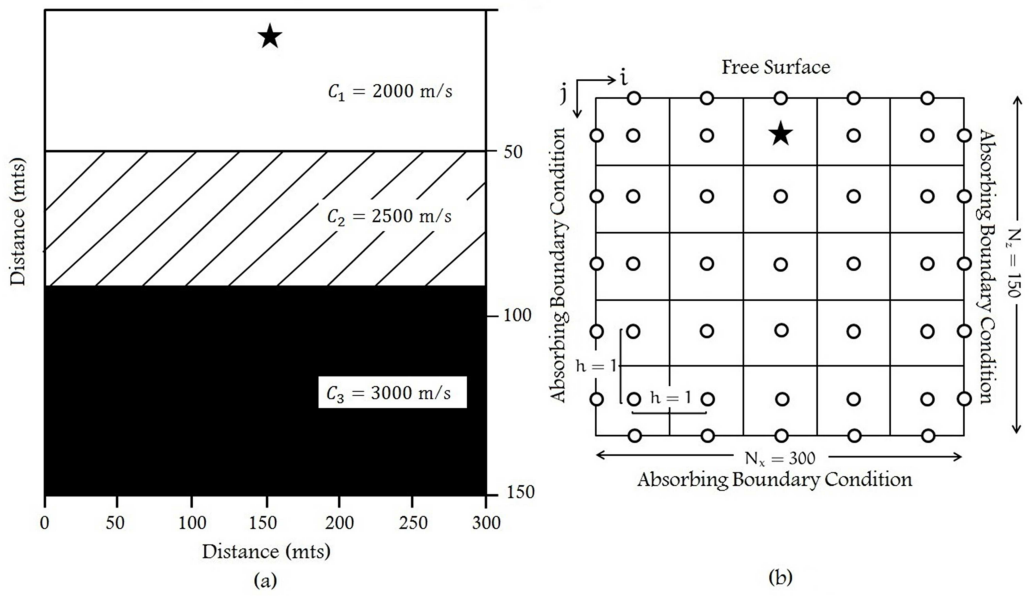

Fig. 6: (a) Velocity model and geometry. (b) Computational region with a staggered grid.

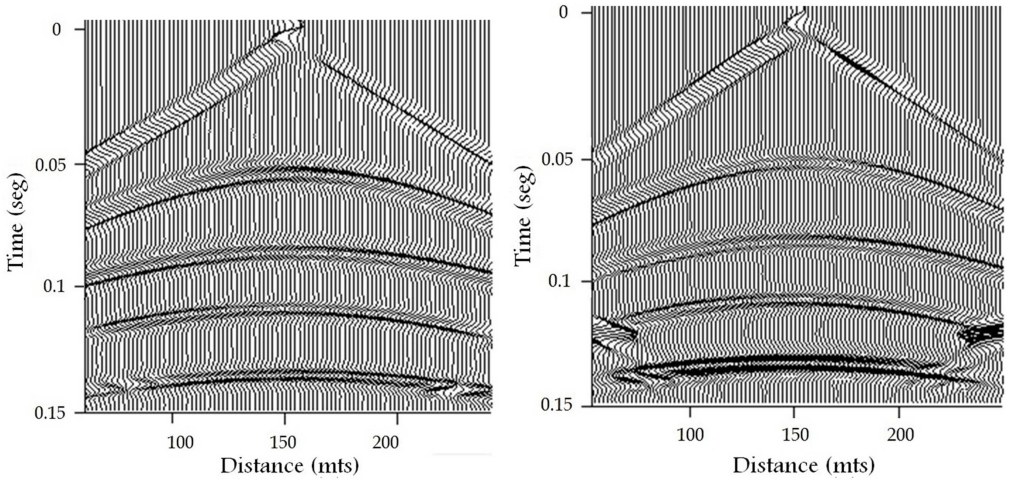

Fig. 7: (a) Seismic traces for absorbing conditions. (b) Seismic traces for Dirichlet conditions.